

Modeling and simulation of CZTS-perovskite sandwiched tandem solar cell

Ismaila Taiwo BELLO, Mojinyinola Kofoworola AWODELE*

Oluwaseun ADEDOKUN, Olusola AKINRINOLA,

Ayodeji Oladiran AWODUGBA

Department of Pure and Applied Physics, Faculty of Pure and Applied Sciences,
Ladoke Akintola University of Technology, Ogbomosho, Nigeria

Received: 26.01.2018

Accepted/Published Online: 09.04.2018

Final Version: 01.06.2018

Abstract: In this research work, a solar cell capacitance simulator (SCAPS-1D) was used in the modeling and simulation of sandwiched perovskite solar cells (PSCs) with a planar heterojunction structure in the arrangement of the sandwiched model (FTO/ZnO/CZTS/PSCS/CZTS/HTM). Two different configurations, 121 and 111, of the sandwiching absorber layer of the device were simulated and compared with the perovskite without sandwiching, using an absorber layer of step length thickness of 25 nm, and varied from 100 nm to 500 nm. The band gap diagram, I-V characteristics curve, and other parameters were constructed. The best configuration for better performance was then determined, from which further simulations were carried out. Efficiency of 22.57% was achieved, which shows that having a combination of two different absorbers was achievable with considerable photon conversion efficiency.

Key words: Perovskite, sandwiched, efficiency

1. Introduction

In the search for more efficient solar cells, an absorbing layer in the solar cells needs to be investigated. The perovskite material is a conventional silicon solar cell. A lead halide perovskite material, $\text{CH}_3\text{NH}_3\text{PbI}_3$, has attracted much attention as an absorbing layer for highly efficient and low-cost solar cells [1–4] with solar cell efficiency boosted from 3% to 20.1% [1–5] and for use in optoelectronic devices, efficient electroluminescence from the visible to NIR range, lasers, and photodetector applications [6,7]. These compounds, which occur in the standard ABX_3 perovskite structure, where A, B, and X are organic cations, e.g., CH_3NH_3^+ , divalent metal cations, e.g., Pb_{+2} or Sn_{+2} , and halogen anions, e.g., Cl-, Br-, or I-, respectively, have a band gap of about 1.55 eV, which can be increased by adding Cl or Br [6–8]. They are materials of low cost due to low temperature solution processing thin-film deposition techniques, which provide polycrystalline films with high charge carrier mobility [9–11].

The last few decades have seen attempts to simulate these important organic materials; in 1986, in a computer simulation of the structure and elastic properties of MgSiO_3 perovskite mineral, a major mantle-forming phase was carried out using computer models that predict the minimum energy structure by using interatomic pair potentials to describe the net forces acting between the atoms [12]. Simulation of the premelting behavior of MgSiO_3 perovskite at high pressures and temperatures was later done using molecular dynamics [13] and computer simulation of defects and diffusion in perovskite SrTiO_3 , CaTiO_3 , and MgSiO_3 was studied later [14].

*Correspondence: mkawodele@lautech.edu.ng

Investigation of perovskite/heterojunction crystalline silicon monolithic tandem solar cells by using device simulation was reported, in which the influence of the conduction and valence band offset between the n-type layer of the perovskite top cell and the tunnel recombination junction was investigated [15], and more recently investigations were carried out for the discovery of Pb-free perovskite solar cells via high-throughput simulation on the K Computer, in which a systematic high-throughput simulation with density functional theory for 11,025 compositions of hybrid organic–inorganic halide compounds in ABX_3 and $A_2BB'X_6$ forms was conducted, where A is an organic or inorganic component, B/B' is a metal atom, and X is a halogen atom. [16]. Attempts to simulate perovskite solar cells analytically have also been on the increase. A physics-based analytical model for perovskite solar cells was investigated [17]. That worked developed a physics-based analytical model to describe the operation of different types of perovskite solar cells, explicitly accounting for nonuniform generation, carrier selective transport layers, and voltage-dependent carrier collection. The model allowed experimentalists to characterize key parameters of existing cells, understand performance bottlenecks, and predict the performance of perovskite-based solar panels, the obvious next step in the evolution of perovskite solar cell technology.

Another interesting and attractive absorber material is $Cu_2ZnSn(S_xSe_{1-x})_4$ (CZTSSe), a chalcogenide absorber in TF solar cells, because it is made of nontoxic (in the case of a pure sulfur-based compound, with no selenium), earth-abundant, and low-cost raw materials and shows high-efficiency potential for the near future [18].

CZTSSe material has an optical absorption coefficient higher than 10^4 cm^{-1} at wavelengths lower than the band gap measured by absorption spectroscopy [19]. This permits it to absorb light with an absorber of very thin thickness (1–2 μm).

We then considered it worthy to simulate a stack containing both perovskite and CZTS materials to act in tandem as an absorber layer.

Simulation of solar cells generally has been much easier as many simulation software models to simulate solar cell devices numerically are freely available. These include AMPS, Silvaco, SCAPS, SimWindows, and AFORS-HET. In this research work, SCAPS software was used to simulate a sandwiched perovskite-based solar cell. SCAPS (Solar Cell Capacitance Simulator) is a one-dimensional simulation program with seven semiconductor input layers developed by a group of photovoltaic researchers at the Department of Electronics and Information Systems, Ghent University, Belgium [20].

2. Materials and methods

2.1. Device structure

The cell model used in the simulation (Figure 1) is a stack of n-FTO/n-ZnO/p-CZTS/p-PSC/p-CZTS/HTM. This cell structure consists of fluorine-doped tin oxide ($Sn_2O:F$) as the transparent conductive layer, an n-type ZnO layer as the buffer layer, a perovskite layer ($CH_3NH_3Pb_{3-x}Cl_x$), and Cu_2ZnSnS_4 (CZTS), which is p-type.

Two different cells considered were 1:2:1 and 1:1:1, which connote the CZTS : PSC : CZTS ratio in the absorber medium, and they were subjected to thickness variation in step lengths of 25 nm. The cell was illuminated through transparent conductive oxide (TCO), which serves as a window layer and passes across the electron transport layer (n-type ZnO), which serves as a buffer layer, and enters the absorber layer to the hole transport material.

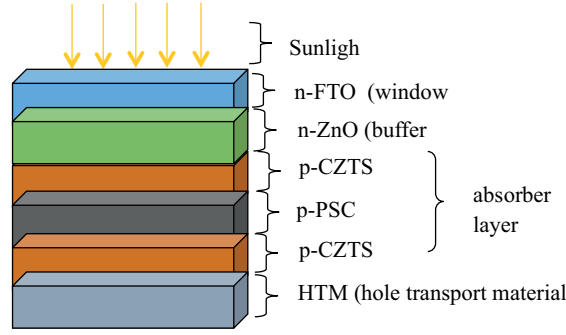


Figure 1. Model of sandwiched simulation structure.

2.2. Simulations

The SCAPS-1D simulator bases its simulations on the solutions of three basic semiconductor equations: Poisson's equation, the continuity equation of electrons, and the continuity equation of holes. SCAPS-1D software solves these three coupled partial differential equations numerically for the electrostatic potentials of electrons and hole concentrations as a function of positions x .

Poisson's equation is given as:

$$\frac{\partial}{\partial x} \left(\varepsilon \frac{\partial \Psi}{\partial x} \right) = \frac{-q}{\varepsilon_0} [p - n + N_D^+ - N_A^- + \frac{\rho def(n, p)}{q}], \quad (1)$$

where ψ is electrostatic potential, ε is the dielectric constant, and q is electronic charge. The first two terms on the right side are free charge carriers per volume while the third and fourth are an ionized donor and acceptor-like dopants, i.e. localized states, and ρdef is defect charge density.

Thus, the conservations of free electrons and free holes in the device are expressed as continuity equations:

$$\frac{\partial n}{\partial t} = -\frac{\partial J_n}{\partial x} + G - U_n(np), \quad (2)$$

$$\frac{\partial p}{\partial t} = -\frac{\partial J_p}{\partial x} + G - U_p(np), \quad (3)$$

where n, p are free carrier concentrations, $N_{D,A}$ are charged dopants, $\rho def(n, p)$ are defect distributions, j_n, j_p are the electron and hole current densities, $U_{n,p}$ are the net recombination rates, and G is the generation rate.

The material parameters sourced from experiments and used in this simulation are given in the Table. The simulator based on the input parameters determined the absorption coefficients of the materials used and the arrangement of the model as allowed by the SCAPS-1D simulator.

Absorber layers were varied while the other parameters were kept constant. Various efficiencies were generated based on the thickness variation of the absorber.

All simulations in this work were performed under ambient temperature (300 K). The electrical parameters (V_{OC} , J_{SC} , FF) and efficiency generated by SCAPS-1D were then used to determine the optimum thickness of the absorber layer in the two configurations.

The current density–voltage (J–V) curves and quantum efficiency (QE) of the best solar cells from the simulation were then determined and the effect of the sandwiching in the absorber layer in the solar cell was investigated.

Table. Material parameters used in simulation.

Parameters	FTO	ZnO	PSC	CZTS
Thickness (μm)	0.5	0.05	Varied	Varied
Band gap (eV)	3.5	3.35	1.55	1.55
Electron affinity (eV)	4.0	4.21	3.9	4.5
Dielectric constant	9	9	6.5	10
Conduction band-DOS $N_c(cm^{-3})$	$2.2 \cdot 10^{18}$	$2.2 \cdot 10^{18}$	$2.2 \cdot 10^{18}$	$2.2 \cdot 10^{18}$
Valence band-DOS $N_v(cm^{-3})$	$1.8 \cdot 10^{19}$	$1.8 \cdot 10^{19}$	$1.8 \cdot 10^{19}$	$1.8 \cdot 10^{19}$
Electron thermal velocity (cm/s)	$1.0 \cdot 10^7$	$1.0 \cdot 10^7$	$3.0 \cdot 10^7$	$1.0 \cdot 10^7$
Hole thermal velocity (cm/s)	$1.0 \cdot 10^7$	$1.0 \cdot 10^7$	$3.0 \cdot 10^7$	$1.0 \cdot 10^7$
Electron mobility ($cm^{-3} V^{-1} s^{-1}$)	2.0	25	1.6	100
Hole mobility ($cm^{-3} V^{-1} s^{-1}$)	1.0	100	0.2	20
Donor density $N_D(cm^{-3})$	$2.0 \cdot 10^{19}$	$1.0 \cdot 10^{18}$	0	0
Acceptor density $N_A(cm^{-3})$	0	0	$6 \cdot 10^{18}$	$8.22 \cdot 10^{18}$

[21,22].

3. Results and discussion

The band diagram of perovskite depends on the compositional variation of the components entailed in the processing and synthesis of the absorber materials, such as organic, metal, and anion composition of the material. The band gap of the absorbing material is a crucial parameter for photovoltaic actions, as the absorber layer is the key material in any solar cell device [23].

Thus, the band alignment is the type II broken band gap with a band gap of approximately 1.55 eV, which is concurrent with the theoretical conditions reported [24]. Figure 2 shows that the band alignment of perovskite solar cells describes a single junction in the band gap while that of the sandwiched perovskite band gap shows three junctions and this confirmed the presence of sandwiching materials embedded within the absorber layer.

3.1. J – V characteristic of simulated device

$J - V$ curves are the parameters used to determine the electrical output power of any solar cells. The curve obtained is shown in Figure 3, where open circuit voltage $V_{OC} = 0.80 V$, short circuit current $J_{SC} = 28.22 mAcm^{-2}$, fill factor $FF = 49.99\%$, and percentage conversion efficiency $PCE = 22.57\%$. These are cell output parameters under the standard simulated sunlight of AM1.5G. The working conditions are at ambient temperature and a frequency of 10^6 Hz.

3.2. Effect of sandwiched absorber layer configuration

Solar cell device performance depends solely on the electrical characteristic and variation of the absorber thickness. Therefore, this work tries to investigate the effect of the combination of the CZTS absorber layer and organometallic (perovskite) layer, embedded in one solar cell. From Figure 4, when the perovskite material thickness in the absorbing layer was 100 nm, the efficiency of the perovskite cells was around 10.52%, while the efficiencies of the sandwiched perovskite with configurations 121 and 111 are 16.12% and 18.99%, respectively, with a percentage increase of 53% and 80%, respectively. At 125 nm thickness, efficiency of 12.01% was observed

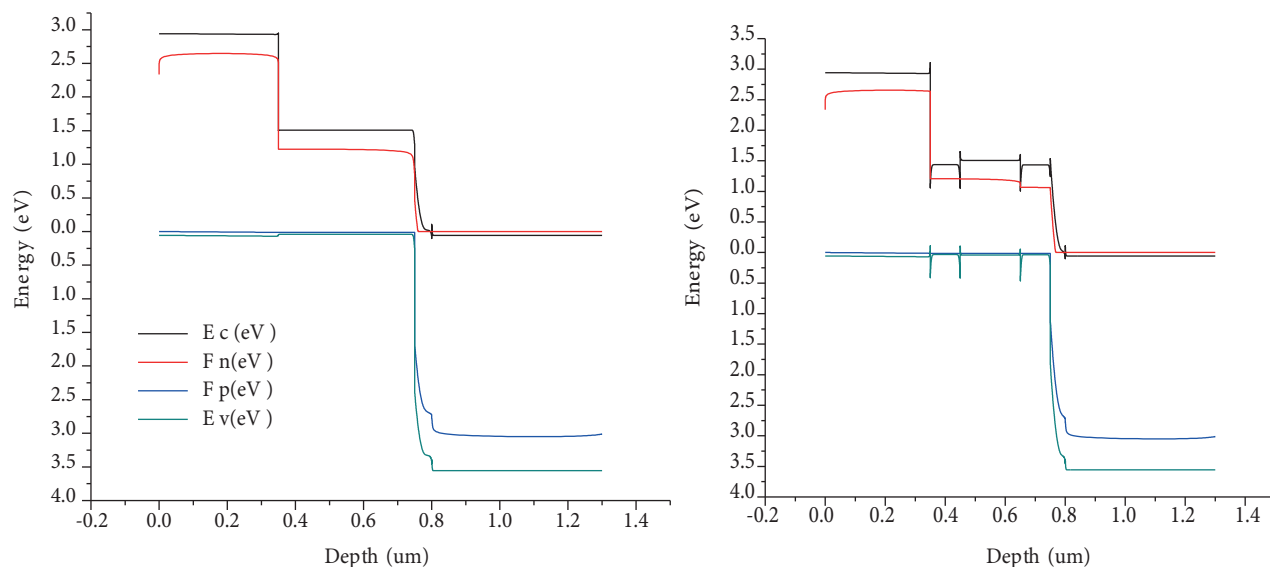


Figure 2. The band diagram of sandwiched perovskite.

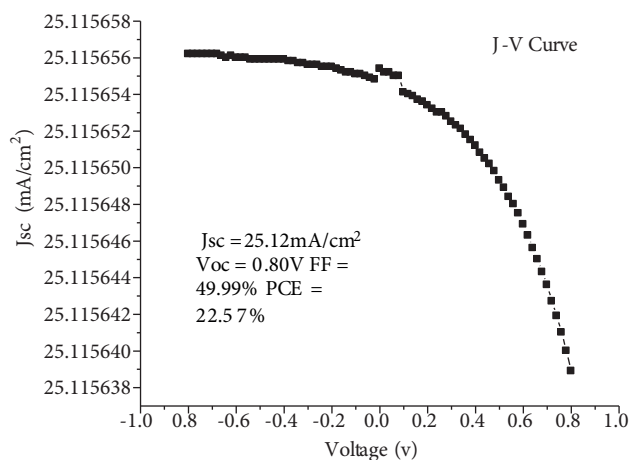


Figure 3. Sandwich $J - V$ curve characteristic.

for perovskite, while 17.59% and 20.14% efficiencies were observed for sandwiched perovskite for 121 and 111 configurations with percentage increases of 46% and 68%, respectively. Efficiency of 13.25% was observed for perovskite solar cells while 18.67% and 20.92% efficiencies were observed for sandwiched perovskite solar cells at 150 nm with percentage increases of 41% and 58%, respectively. At 175 nm, efficiency of 14.29% was observed for perovskite, while 19.48% and 21.46% efficiencies were observed for sandwiched perovskite cells with percentage increases of 36% and 50%, respectively. At 200 nm, 15.16% efficiency was observed for perovskite cells, while efficiency of 20.09% was observed for the 121 configuration and 21.86% for the 111 configuration with percentage increases of 33% and 44%, respectively. However, 15.90% efficiency was recorded for perovskite cells while 20.57% and 22.15% efficiencies were observed at 225 nm for sandwiched perovskite solar cells, respectively, with percentage increments of 29% and 39%. At 250 nm, efficiency of 16.52% was observed for perovskite and 20.95% and 22.39% efficiencies were observed for sandwiched perovskite cells with percentage increases of 27% and 36%, respectively. Efficiency of 17.05% was observed for perovskite while 21.26% and 22.57% efficiencies

were recorded for sandwiched solar cells with percentage increases of 25% and 32%, respectively, at 275 nm thickness. At 300 nm, efficiency of 17.51% was observed for perovskite solar cells, while 21.51% and 22.72% were observed for sandwiched Perovskite cells with percentage increases of 23% and 30%. Efficiency of 17.90% was recorded for the Perovskite cells at 325 nm while the efficiencies of sandwiched perovskite cells were observed to be 21.72% and 22.85% with percentage increases of 21% and 28%, respectively. At 350 nm, 18.24% efficiency was observed for perovskite while 21.90% was observed for 121 sandwiching Perovskite with a percentage increase of 20%. However, in the 111 configuration, it was noted that convergence failure calculated for $V = 0.000$ V was observed, which shows that 325 nm is the optimum thickness for sandwiched perovskite solar cells. The 111 configuration is cut off in Figure 4, implying that the configuration has large bandwidth, which affects the absorption processes to create electron-hole pairs for the excitation of photons.

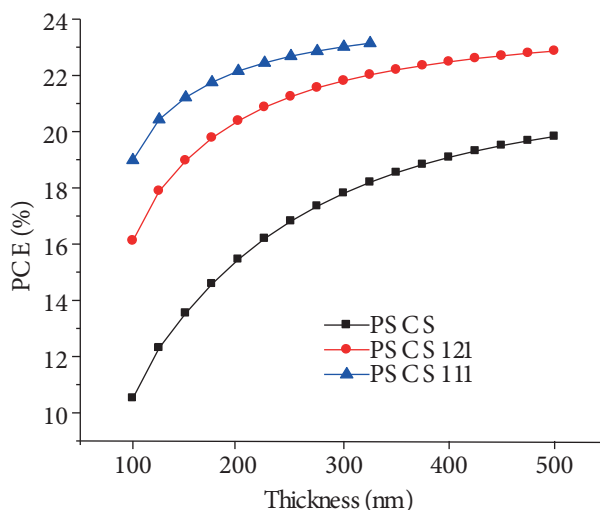


Figure 4. Sandwiched percentage conversion efficiency against thickness.

Meanwhile, at 375 nm, efficiency of 18.53% was recorded for perovskite solar cells, while 22.05% was observed for sandwiched perovskite with a percentage increase of 19%. At 400 nm efficiencies of 18.79% and 22.18% were recorded for perovskite and sandwiched perovskite solar cells with percentage increases of 18%. At 425 nm, efficiency of 19.01% was observed for perovskite solar cells, while 22.30% was observed for the sandwiched perovskite with a percentage increase of 17%. At 450 nm, 19.21% and 22.40% efficiencies were observed for perovskite and sandwiched perovskite solar cells, respectively, with a percentage increase of 17%. However, 19.38% and 22.49% efficiencies were observed for perovskite and sandwiched perovskite, respectively, at 475 nm with a percentage increase of 16%. Lastly, at 500 nm, the efficiency of perovskite was observed to be 19.53% and that of sandwiched perovskite was around 22.57%, with a percentage increase of 16%. Thus, there is no appreciable increment in the percentage increases of the efficiency values of sandwiched perovskite from 425 nm thickness of absorber layers. However, any further simulation beyond 500 nm in the 121 configuration failed as there was no convergence. Simulations thus could not go beyond 500 nm for sandwiched perovskite solar cells using the 121 configuration.

3.3. Quantum efficiency of the solar cell

The quantum efficiency may be given either as a function of wavelength or as energy. Figure 5 shows the plot of quantum efficiency against the wavelength, which showed that more than 90% of the wavelength between

300 nm and 890 nm radioactively recombined, and less than 10% of such wavelength recombined through other processes (Auger and SRH).

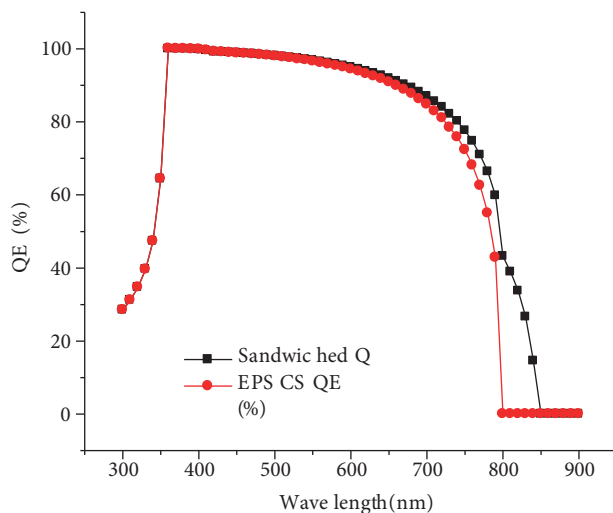


Figure 5. PSCS and sandwiched QE against wavelength.

This implied that, at 500 nm thickness, the sandwiched layer absorbs almost all the incident photons to create the electron–hole pairs and the photogenerated carriers by built-in field with minimum recombination.

Figure 5 shows that the sandwiched layer can absorb incident photons up to 800 nm, which implies that the sandwiched absorber layer can perform better than the perovskite layer, which can only absorb photons around 750 nm, because the higher the wavelength, the lower the photon energy. Meanwhile, the flattening out of the curve at 800 nm shows that there would not be any absorption beyond the region.

4. Conclusion

Perovskite and sandwiched perovskite-based solar cells have been successfully simulated using SCAPS-1D. It was observed that with increment in the absorber layer thickness from 100 to 500 nm, the efficiencies of sandwiched perovskite solar cells were increased appreciably (with optimum 80% at 500 nm) compared to ordinary perovskite solar cells. It was found also that higher absorber thicknesses up to 400 nm had higher efficiencies and other electrical outputs of the solar cell. Efficiencies of 19.53% and 22.57% were recorded for the perovskite and sandwiched perovskite-based solar cells, respectively. Thus, the appreciable increment in the efficiency values of sandwiched perovskite solar cells showed the positive performance of the sandwiching absorber layer.

Acknowledgments

The authors thank Dr Marc Burgelman and his colleagues at Ghent University, Belgium, for making SCAPS-1D available for use. One of the authors also thanks the TETFUND for a grant used in this work and others.

References

- [1] Lee, M. M.; Teuscher, J.; Miyasaka, T.; Murakami, T. N.; Snaith, H. J. *Science* **2012**, *338*, 643-647.
- [2] Burschka, J.; Pellet, N.; Moon, S. J.; Humphry-Baker, R.; Gao, P.; Nazeeruddin, M. K.; Gratzel M. *Nature* **2013**, *499*, 316-319.

- [3] Liu, M.; Johnston, M. B.; Snaith, H. J. *Nature* **2013**, *501*, 395-398.
- [4] Gratzel, M. *Nat. Mater.* **2014**, *13*, 838-842.
- [5] Suarez, B.; Gonzalez-Pedro, V.; Ripolles, T. S.; Sanchez, R. S.; Otero, L.; Mora-Sero, I. *J. Phys. Chem. Lett.* **2014**, *5*, 1628-1635.
- [6] Deschler, F.; Price, M.; Pathak, S.; Klintberg, L. E.; Jarausch, D. D.; Higler, R.; Huttner, S.; Leijtens, T.; Stranks, S. D.; Snaith, H. J. et al. *J. Phys. Chem. Lett.* **2014**, *5*, 1421-1426.
- [7] Xing, G.; Mathews, N.; Lim, S. S.; Yantara, N.; Liu X.; Sabba, D.; Gratzel, M.; Mhaisalkar, S.; Sum, T. C. *Nat. Mater.* **2014**, *13*, 476-480.
- [8] Zhou, H.; Chen, Q.; Li, G.; Luo, S.; Song, T. B.; Duan, H. S.; Hong, Z.; You, J.; Liu, Y.; Yang, Y. *Science* **2014**, *345*, 542-546.
- [9] Su, L.; Zhao, Z. X.; Li, H. Y.; Yuan, J.; Wang, Z. L.; Cao, G. Z.; Zhu, G. *ACS Nano* **2015**, *9*, 11310-11316.
- [10] Yakunin, S.; Sytnyk, M.; Kriegner, D.; Shrestha, S.; Richter, M.; Matt, G. J.;
- [11] Azimi, H.; Brabec, C. J.; Stangl J.; Kovalenko, M. V. et al. *Nat. Phot.* **2015**, *9*, 444-449.
- [12] Kumawat, N. K.; Dey, A.; Narasimhan, K. L.; Kabra, D. *ACS Phot.* **2015**, *2*, 349-354.
- [13] Wall, A.; Price, G. D.; Parker, S. C. *Mineral. Mag.* **1986**, *50*, 693-707.
- [14] Matsui, M.; Price, G. D. *Nat.* **1991**, *351*, 735-737.
- [15] Wright, K.; Price, G. D. *J. Geophys. Res.* **1993**, *98*, 22245-22253.
- [16] Karki, B. B.; Khanduja, G. *Model. Simul. Mater. Sc.* **2006**, *14*, 1041.
- [17] Nakajima, T.; Sawada, K. *J. Phys. Chem. Lett.* **2017**, *8*, 4826-4831.
- [18] Nakanishi, A.; Takiguchi, Y.; Miyajima, S. *Appl. Mater. Sci.* **2016**, *213*, 1997-2002.
- [19] Ki, W.; Hillhouse, H. W. *Adv. Energy Mater.* **2011**, *1*, 732-735.
- [20] Katagiri, H.; Jimbo, K.; Maw, W. S.; Oishi, K.; Yamazaki, M.; Araki, H.; Takeuchi, A. *Thin Solid Films* **2009**, *517*, 2455-2460.
- [21] Niemegeers, A.; Burgelman, M.; Decock, K.; Verschraegen, S.; Degrave, S. *SCAPS Manual, Version 2*; Ghent University: Ghent, Belgium, 2013.
- [22] Takashi, M.; Masashi, M. *J. Appl. Phys.* **2014**, *116*, 054505.
- [23] Gloeckler, M.; Fahrenbruch, A. L.; Sites, J. R. In *3rd World Conference Proceedings: Photovoltaic Energy Conversion*; Osaka, Japan, 2003.
- [24] Fonash, S. J. *Solar Cell Device Physics*, 2nd ed.; Elsevier: New York, NY, USA, 2010.
- [25] Shockley, W.; Queisser, H. *J. Appl. Phys.* **1961**, *32*, 510.